Towards emission enhancement of blue emitters in hBN using plasmonic lattices

Karin Yamamura[1,2†], Shu An[3†], Ivan Zhigulin[1], Mehran Kianinia[1,2], Yiming Wu[3] , Zhaogang Dong[3,4.] *, Igor Aharonovich[1,2,] *

[1] School of Mathematical and Physical Sciences, University of Technology Sydney, Ultimo, New South Wales 2007, Australia
[2] ARC Centre of Excellence for Transformative Meta-Optical Systems, University of Technology Sydney, Ultimo, New South Wales 2007, Australia
[3] Institute of Materials Research and Engineering (IMRE), Agency for Science Technology and Research (A*STAR), 2 Fusionopolis Way, Innovis #08-03, Singapore 138634, Republic of Singapore
[4] Science, Mathematics, and Technology (SMT), Singapore University of Technology and Design (SUTD), 8 Somapah Road, Singapore 487372

† These authors contributed equally to this work.

* To whom correspondence should be addressed: Zhaogang Dong (Zhaogang_Dong@sutd.edu.sg) and Igor Aharonovich (Igor.Aharonovich@uts.edu.au)

Abstract

Hexagonal boron nitride (hBN) has been gaining attention as a compelling material platform hosting quantum emitters at room temperature. A particularly important family of emitters in hBN are those with a zero phonon line at 436 nm (termed B-Centres) since these can be engineered on demand using electron beam irradiation. In this work, we demonstrate a pathway to integrate these emitters with plasmonic lattices. The blue wavelength necessitates the use of aluminium metal, instead of gold or silver. Consequently, we utilise trench cavity geometry and transfer hBN layers on top of the lattice. We then create deterministically the emitters and measure a six-fold enhancement in the emission intensity. We conclude by discussing the potential possibilities of the plasmonic lattice arrays for scalable enhancement of quantum emitters in layered materials.

Keywords: hexagonal boron nitride, Single photon emitter, van der Waals materials, plasmonic gap cavities, B-centre

Introduction

Solid-state single photon emitters (SPEs) from defects in wide bandgap materials are attracting a great amount of attention due to their robust operation at room temperatures[1, 2]. Hexagonal boron nitride (hBN) stands out as a particularly attractive candidate for hosting SPEs[3, 4]. This material demonstrated the ability to support a large wavelength range of SPEs, extending from ultraviolet to near-infrared spectrum, with narrowband emission and fast

fluorescence lifetimes[5-12]. In addition, the van der Waals crystalline property of hBN allows for sub-nanometer thickness single layer exfoliation, suitable for new generation of optoelectronic devices[13].

Among the diverse range of hBN SPEs, a recently emerged defect termed B-Centre has been of a particular interest in the field and is the focus of this work. Exciting properties of the B-Centre include its zero phonon line (ZPL) that is consistently positioned at 436 nm[8, 14-18]. Another key advantage of this particular defect is the ability to deterministically engineer them with low energy (~ sub 30 keV) electron beams. This facilitates great position control and has been utilised to study these emitters for light - matter interactions in cavities and resonators[19] as well as exploring their advanced quantum properties including photon indistinguishability[16].

A key prerequisite for deployment of these SPEs in practical applications is enhancement of their spontaneous photon emission rates[20]. Broadly, there are two distinct pathways to achieve that: Either coupling to a high Q dielectric photonic crystal cavity, which is often challenging and requires sophisticated nanofabrication[21]; Or coupling to a metallic plasmonic cavity, that often enables much stronger light localisation and broader resonances. For the latter, the intense local electromagnetic field and confinement of subwavelength modes facilitated by the plasmonic gap can lead to ultrafast emission rates, and enhance both excitation and spontaneous emission rates, resulting in increased fluorescence rates[22-25].

Earlier works on plasmonic enhancement of visible SPEs in hBN, employed gold or silver based plasmonic resonators[26-30]. However, these materials are not suitable for the blue spectral range, where the B-Centre emission is located. Aluminium (Al) is expected to be a candidate as a plasmonic material from the UV to the visible range[31, 32]. Key features of Al include its minimal intrinsic losses at this spectral range and the ability to deposit high quality thin layers with smooth surface. Notably, however, while Al plasmonics have been studied for a few years, coupling quantum emitters to Al resonators so far remained elusive.

In this work, we demonstrate plasmonic coupling of the B-Centres in hBN to an Al made plasmonic lattice[33, 34]. We design and engineer plasmonic lattice with horizontal nanotrench cavities, with resonances at the 436 nm range, to match with the ZPL of the blue emitters. We observe a modest six-fold enhancement in emission, and discuss the potential applications with these lattices.

Results and Discussion

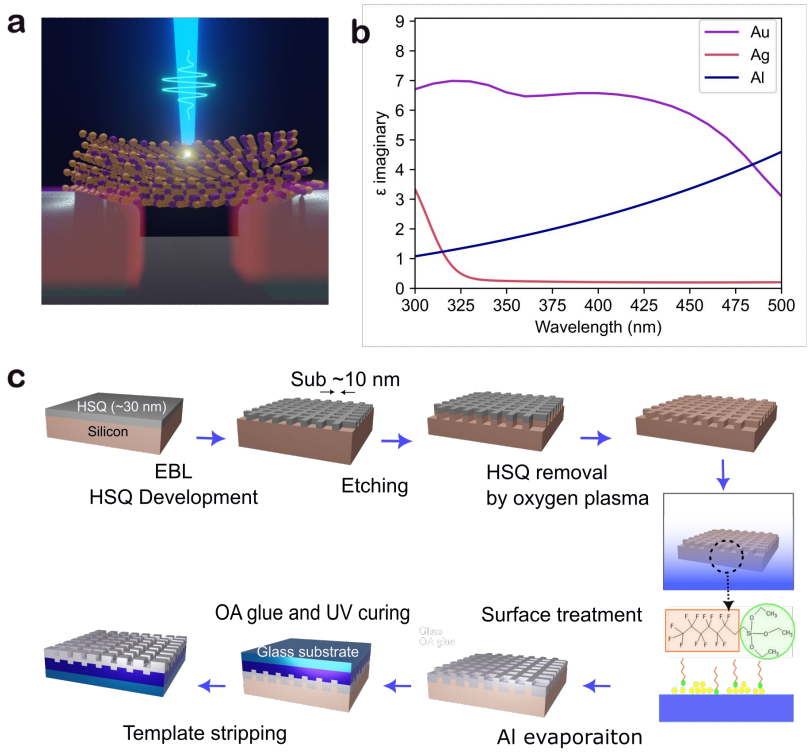

Fig 1. *(a) Schematic illustration of the hBN hosting the B-Centre coupled to a plasmonic nanotrench cavity. (b)The imaginary part of permittivity of gold (Au), Aluminum(Al) and silver (Ag). (c) Schematics of the fabrication process of the plasmonic cavities using template-stripping method. In brief, hydrogen silsesquioxane (HSQ) is deposited on a silicon (Si) substrate, and the nanotrench array is patterned by an EBL, and subsequently etched down using reactive ion etching. After deposition of a 100 nm of Al, a glass substrate is glued on top, and subsequently, template stripped from the original Si wafer. The surface treatment before Al deposition allows for stripping of the nanotrench from Si substrate.*

Enhanced emission from coupled emitters to a plasmonic nanostructure can be achieved through combination of purcell enhancement and improved excitation and collection efficiency. This is schematically shown in figure 1(a) for the B-Centres in hBN. Figure 1(b) compared the permittivity of aluminium, gold and silver in the blue region (400-500 nm)[35]. It indicates that the imaginary part of the permittivity of Al is lower than that of Au.

To fabricate the nanotrench Al plasmonic array, a template stripping approach was employed. A Si substrate has been used as a template. To achieve the small feature size required for the nanotrench, a 80 nm 6% hydrogen silsesquioxane (HSQ) mask is deposited on top of the Si substrate. It is then patterned using electron beam lithography (EBL). The pattern is then transferred into the Si substrate by chlorine (Cl2) and HBr gases-based reactive ion etching (RIE). The remaining resist is removed in oxygen plasma. To create a monolayer for stripping off the template, the patterned Si is immersed in a diluted solution of

1H,1H,2H,2H-Perfluorodecyltriethoxysilane for several hours. Then, a 100 nm layer of Al is deposited using an E-beam evaporator which is then attached to a glass substrate using organic adhesive (OA) glue. Finally, After 20 minutes of annealing, the Si template is removed to get the Al nanotrench on the glass. The nanotrench fabrication steps are shown schematically in figure 1(c).

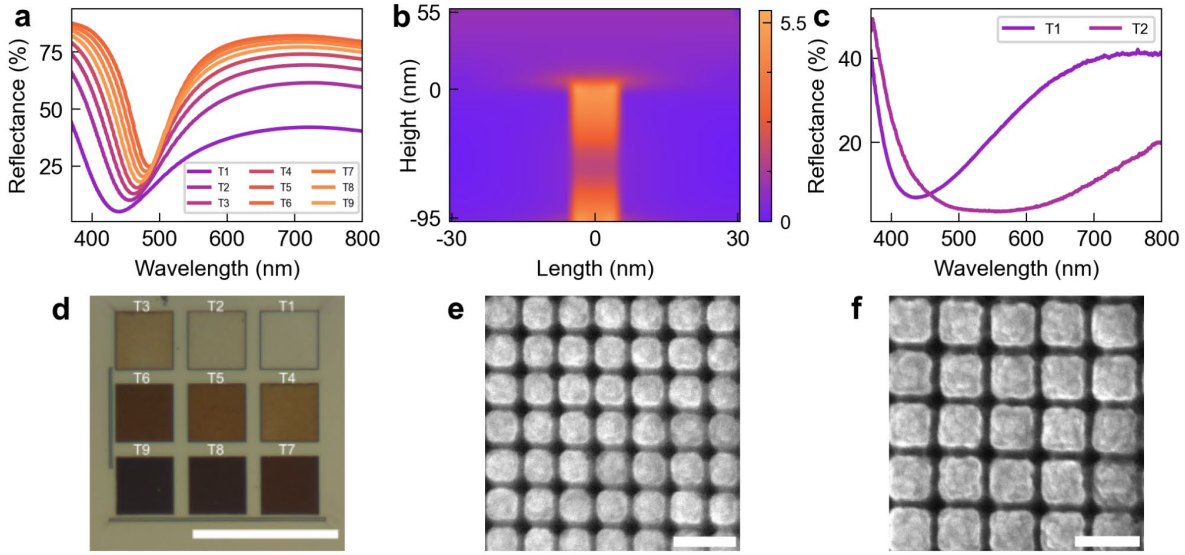

Fig. 2 *(a) Numerical simulation of reflectance with respect to y-polarisation corresponding to nanotrenches with different pitch width ranges in 60 - 220 nm (T1 - T9) and (b) Electric field distribution of T1 with pitch of 60 nm under incident light y-polarisation showing the strong field between Al nano trenches up to 10 nm above the surface. (c) Experimental reflectance measurement of T1 and T2 with pitch of 220 nm and 200 nm, respectively. (d) Optical image of the fabricated nanotrenches labelled T1 to T9. The scale bar is 50 µm. (e, f) SEM images from nanotrenches T1 (T2), with pitch sizes of 60 nm (80 nm), respectively. The scale bar is 100 nm.*

The fabricated structures were modelled using a finite-difference time-domain (FDTD) simulator (Lumerical) to optimise the absorbance around the emission of the B-Centre at 436 nm. We simulated reflectances of the Al nanotrenches with different pitch sizes ranging from 60 nm to 220 nm with 20 nm steps, for trenches T1 - T9, respectively, as shown in figure 2a. The reflectance spectra show the lowest reflectance in T1 at 436 nm, following that, we simulated the electric field distribution of T1 under incident light with respect to the y-polarisation, as shown in figure 2b. The scale on the left shows the electric field enhancement factor, which is proportional to the Purcell factor. The electric field within the gap and up to 10 nm above the Al surface reaches the highest enhancement factor of 5.5 compared to the Al surface itself. The highest electric field is in the trench between the Al nanostructures, and approximately within 10 nm range above the surface. The native oxide layer on as-evaporated Al is around 2 nm. We have added a 2 nm thick Al_2O_3 layer on top of

the Al layer in the simulation model and found that the reflection dip was only systematically red-shifted by 2-3 nm with a slight increase in reflection dip intensity. Therefore, the effect of the oxidation layer can be ignored in the simulation and experiment. To confirm our simulation result we have added the measured reflectance of T1 and T2 trenches (shown in figure 2(c)). The reflectance measurement result of T1 agrees with the simulation results supporting plasmonic modes around ZPL wavelength of B-Centres in hBN. The spectra of T2 shows a red-shift and a broader, lower reflectance for a wider wavelength range from 400-800 nm. It could be due to edge effect and round corners in the fabricated Al nanotrenches. The Al nanotrenches were designed to have low reflectance at the B-centre ZPL of 436 nm, making T1 and T2 suitable for coupling B-centres to the plasmonic lattices.

The fabricated sample consists of plasmonic nanostructures with nine different pitch sizes on a glass, as shown optically in figure 2d. Each array is approximately 25 x 25 μm^2 in size. Figures 2(e, f) show high magnification scanning electron microscope (SEM) images of the aluminium nanotrenches labelled T1 and T2 with pitch sizes of 60 nm and 80 nm, respectively. The lattices exhibit nanoscale gap trenches that act as the plasmonic cavities for the enhancement of the emission.

After the fabrication of the plasmonic lattice, we transferred a hBN flake (~ 50 nm thick) onto the lattice and pressed firmly to ensure the flake has a good contact to the plasmonic lattices. To verify the surface profile, we captured an AFM image, which confirmed that the hBN flake bends toward the plasmonic lattice grooves, indicating good contact with the structure (shown in figure S1). Figure 3(a) shows the optical image of the hBN flake after it was transferred on top of the plasmonic lattice. A photoluminescence (PL) confocal map of hBN after the transfer (figure 3(b)) shows no emission within the spectral range of blue emitters. This is further confirmed by acquiring the spectra from 425 nm to 480 nm range as shown in figure 3(c). The PL background signal due to the plasmonic lattices was not affected by the addition of transferring the hBN flake on the plasmonic structure.

To generate B-Centres in the hBN flake, a SEM microscope with a 5 keV electron beam acceleration voltage was employed. Although electron beam irradiation is effective in generation of blue emitters, exact alignment of the irradiation spots with the nanoscale trenches presented a significant challenge. To overcome this issue, we implemented irradiation of lines and rectangular patterns to create the B-Centres. This broad irradiation enables simultaneous creation of a homogeneous ensemble of B-Centres, as well as an overlap with the plasmonic nanotrenches. We specifically targeted trenches T1 and T2 as their plasmonic lattices match closely the B-Centre emission.

Figure 3(d) shows the PL spectra of the formed B-Centres on T1 -T9 lattices except T7 since hBN flake is not integrated on T7 due to the size of the flake. Both spectra on T1 and T2 show characteristic to B-Centre emissions of the ZPL at ~ 436 nm and the phonon sideband at ~ 465 nm (shown in figure 3(d) inset). Spectra on other lattices show a large background signal. Various factors such as emitters dipole, the position of emitters relative to the trench affect the coupling efficiency of these emitters to the plasmonic structure. The fabrication

method provides control of the lateral position, however, the vertical placement of B-Centres as well as their emission dipole with respect to the plasmonic lattice remain uncontrolled. In addition, the plasmonic structure couples to an in-plane dipole in the direction of the gap. B centres in hBN have been shown to have in-plane dipole but are randomly oriented within hBN flake. In this case, created emitters are fully or partially aligned with the nano trench randomly, resulting in different coupling efficiencies.

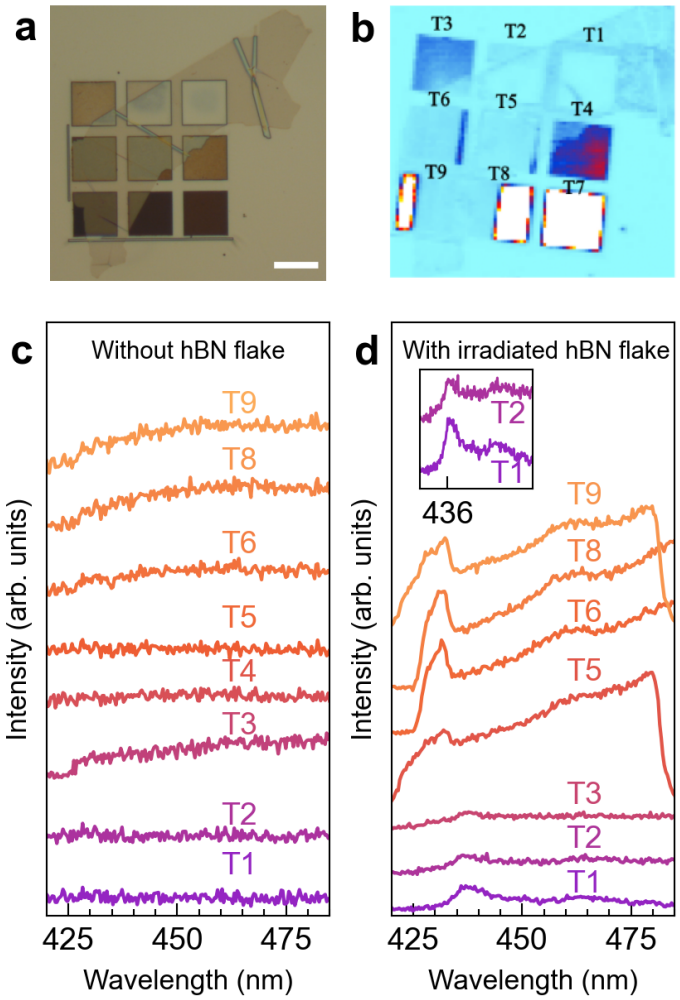

Fig 3. *(a) Optical image of the transferred hBN flake onto the nano trench lattices. The scale bar is 20 µm. (b) PL map of the Al plasmonic lattices with the hBN flake. PL spectra of the plasmonic lattices (c) and (d) after irradiation of the hBN to create B-Centres. The inset shows PL spectra of irradiated hBN on T1 and T2 with clear emission at 436nm (B center ZPL). The emission at 428nm is hBN raman.*

To investigate the enhancement of the emission on the T1 nano trench array (that overlaps the most with the ZPL of the B-Centre), we collected emission along the irradiated

line. The irradiated region was chosen along the nanotrench area during the electron irradiation with SEM so that the created emitters are positioned within the nanotrench. Under the PL scan, we found multiple spots containing B center emission, numbered from S1 to S8 here. The spectra from these spots are shown in figure 4(a). The PL spectra were acquired at the highest intensity for each emitter by carefully adjusting the focus. For each emitter, spectra collection was carried out using a 460 nm ± 30 nm bandpass filter with an integration time of 20 seconds. The spectra were fitted with a Lorentzian function centred at the ZPL at 436 nm to compare the maximum photon counts per second for each emitter. There is no emission enhancement for most of the emitters except those on positions S7 and S8. This is likely because spots S1-S6 are not overlapping with the individual plasmonic nanotrenches, while S7 and S8 are likely positioned directly above the nanotrench. The intensity variation between S7 and S8 can originate from polarisation and/or vertical location of the emission. Overall enhancements of approximately six fold, in their photon counts at the ZPL compared to uncoupled emitters, are achieved for these two locations. We attribute this emission enhancement due to plasmonic coupling of B-centre with lattice. In order to confirm this, we compared the decay rate of the emission from coupled and uncoupled emitters. Figure 4 (b and c) shows the lifetime from emitters on T1 with 31k and 10k photon counts on APD, and the lifetime were 1.11 ns and 1.83 ns respectively. The lifetime of typical B-centres in hBN ranges from 1.83 to 2.6 ns[17]. The radiative decay rate improvement of the emitter with higher photon counts indicates moderate plasmonic-assisted emission enhancement.

Significant improvement in achieving better coupling between the emitters and the nanotrenches can be realised by engineering emitters in thin hBN flakes, below 10 nm thickness. This would result in a greater overlap probability between emitter location and the high field of the plasmonic trenches. By overcoming this challenge, higher chances of plasmonic enhancement are expected as all emitters would be located at the maximum electric field where highest enhancement is expected.

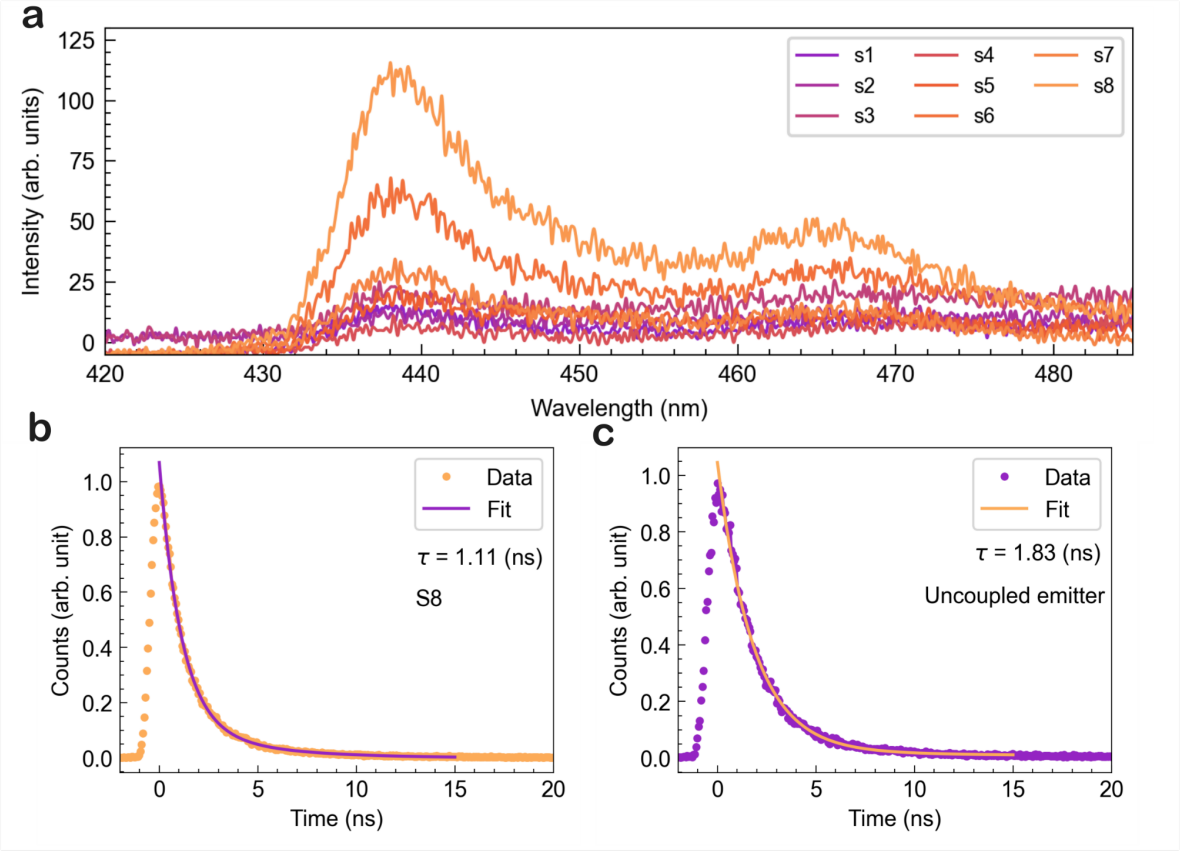

Fig 4. *(a) PL spectra of the B-Centres located on top of the T1 lattice. Enhancement is observed for spots S7 and S8, likely due to the overlap of the formed emitters and the nanotrench. Lifetime measurement of blue emitters with different brightness (b) on S8 with brightest Pl emission and (c) lifetime of emitters with average emission such as S1-S6.*

Conclusion

To conclude, we attempted coupling of the B-Centres with plasmonic lattices. We designed and fabricated Al nanotrench lattices with resonances approaching the blue spectral range. We demonstrated a six-fold increase in PL emission and an improvement in the radiative decay time assisted by plasmonic coupling from the site-specifically fabricated B-Centres. Our research has the potential to explore opportunities for utilising plasmonic enhancement between Al nanostructures and quantum emitters in 2D materials, specifically in the shorter wavelengths where standard plasmonic materials are not suitable.

Methods

Numerical simulation for designing aluminium nanotrench

The simulated reflectance and electric field distribution were obtained using a finite-difference time-domain (FDTD) simulator (Lumerical). The geometries of Al nano trenches in the simulation model were designed based on the SEM image shown in Figure2(e) (pitch of

60 nm and trench width of 10 nm) with a trench depth of 100 nm. The Al nanotrench was placed in a unit cell of 60 nm × 60 nm × 800 nm with a mech of 2 nm × 2 nm × 5 nm around them. In the unit cell, periodic boundary conditions were adopted in both the x and y axis, while perfect match layer (PML) was applied in the z direction. To obtain the reflectance, one monitor was added between the Al nanotenches and y-polarised incident light source with a wavelength range from 350 to 800 nm. The refractive index (n) and extinction coefficient (k) of Al were taken from the software database, while that of hBN is taken from previous experiments[34].

Fabrication of aluminium nanotrenches

First, 6% hydrogen silsesquioxane (HSQ) dissolved in methyl isobutyl ketone (MIBK) was spin coated onto a thoroughly cleaned Si substrate at a speed of 5000 rounds per minute (rpm) for 90 s. The thickness of the HSQ layer was measured to be 80 nm. After that, the patterning was carried out using EBL with an electron acceleration voltage of 100 keV. The exposed HSQ-coated Si sample was then developed and the pattern was transferred to the Si substrate to complete the fabrication of the template. Oxygen plasma treatment was subsequently performed to remove the remaining HSQ. The HSQ-free Si template was then put in diluted 1H,1H,2H,2H-Perfluorodecyltriethoxysilane solution (10 µL in 50 mL toluene) for 2-3 hours to generate monolayer molecular layer on the surface of Si template. A subsequent functionalization via a sol-gel technique using perfluorsilanes leads to superoleophobic surfaces. 100 nm Al was then evaporated on the processed template using e-beam evaporation. Appropriate amount of OA glue was subsequently dropped on as-fabricated Si template, followed by a flip cover of glass substrate (25 mm^2). Finally, the Si template was removed after 20 minutes annealing to get the Al nanotrench on a glass substrate. The reflection spectra were measured using a CRAIC UV-vis-NIR microspectrometer with a 5x objective lens, where we are able to measure the localized reflectance spectra from a patterned area size of 10 µm x 10 µm. The measurement spectrum is normalized to a NIST certified mirror with a well-calibrated absolution reflectance spectrum.

Emitter engineering

hBN flakes were exfoliated from hBN crystal provided by the National Institute for Materials Science (NIMS) using scotch tape and transferred to the cleaned SiO substrate. The thickness of the sample was measured using the atomic force microscope Park XE7 AFM and 4XC-NN AFM tip. The hBN flake was transferred on the glass substrate with Al plasmonic structures using the dry transfer method with polymer stamp. The hBN flake was picked up from the SiO substrate with the polymer stamp and then pressed firmly on the Al nano-trenches. After the transfer, the sample was placed in a beaker with acetone for 5 minutes to remove the excess polymer on the surface of the sample. The sample was irradiated with an electron beam at a voltage of 5 kV and a current of 3.2 nA using Helios G4 PFIB UXe DualBeam.

PL measurements

The optical measurements are conducted using a home-built confocal microscope with a 405 nm CW laser (PiL040X, A.L.S. GmbH) and a 402 nm pulsed laser. Delivered laser power was measured before the objective (Nikon TU Plan Fluor 100x/0.90 NA).

Acknowledgments

This research is supported by the Australian Research Council (CE200100010, FT220100053) and the Office of Naval Research Global (N62909-22-1-2028). The authors thank the ANFF node of UTS for access to facilities.

Z.D. would like to acknowledge the funding support from the Agency for Science, Technology and Research (A*STAR) under its AME IRG (Project No. A20E5c0093), CareerDevelopment Award grant (Project No. C210112019), MTC IRG (ProjectNo. M21K2c0116 and M22K2c0088), the Quantum Engineering Programme 2.0 (Award No. NRF2021-QEP2-03-P09) and DELTA-Q 2.0(Project No. C230917001). The authors acknowledge the ANFF node of UTS for access to facilities.

References

1. Atatüre, M.; Englund, D.; Vamivakas, N.; Lee, S.-Y.; Wrachtrup, J., Material platforms for spin-based photonic quantum technologies. *Nature Reviews Materials* **2018,** *3* (5), 38-51.
2. Ruf, M.; Wan, N. H.; Choi, H.; Englund, D.; Hanson, R., Quantum networks based on color centers in diamond. *J. Appl. Phys.* **2021,** *130* (7), 070901.
3. Aharonovich, I.; Tetienne, J.-P.; Toth, M., Quantum Emitters in Hexagonal Boron Nitride. *Nano Lett.* **2022,** *22* (23), 9227-9235.
4. Kubanek, A., Coherent Quantum Emitters in Hexagonal Boron Nitride. *Advanced Quantum Technologies* **2022,** *5* (9), 2200009.
5. Bourrellier, R.; Meuret, S.; Tararan, A.; Stéphan, O.; Kociak, M.; Tizei, L. H. G.; Zobelli, A., Bright UV Single Photon Emission at Point Defects in h-BN. *Nano Lett.* **2016,** *16* (7), 4317-4321.
6. Stewart, J. C.; Fan, Y.; Danial, J. S. H.; Goetz, A.; Prasad, A. S.; Burton, O. J.; Alexander-Webber, J. A.; Lee, S. F.; Skoff, S. M.; Babenko, V.; Hofmann, S., Quantum Emitter Localization in Layer-Engineered Hexagonal Boron Nitride. *ACS Nano* **2021,** *15* (8), 13591-13603.
7. Ronceray, N.; You, Y.; Glushkov, E.; Lihter, M.; Rehl, B.; Chen, T.-H.; Nam, G.-H.; Borza, F.; Watanabe, K.; Taniguchi, T.; Roke, S.; Keerthi, A.; Comtet, J.; Radha, B.; Radenovic, A., Liquid-activated quantum emission from pristine hexagonal boron nitride for nanofluidic sensing. *Nature Mater.* **2023,** *22* (10), 1236-1242.
8. Fournier, C.; Plaud, A.; Roux, S.; Pierret, A.; Rosticher, M.; Watanabe, K.; Taniguchi, T.; Buil, S.; Quélin, X.; Barjon, J.; Hermier, J.-P.; Delteil, A., Position-controlled quantum emitters with reproducible emission wavelength in hexagonal boron nitride. *Nat. Commun.* **2021,** *12* (1), 3779.
9. Li, C.; Mendelson, N.; Ritika, R.; Chen, Y.; Xu, Z.-Q.; Toth, M.; Aharonovich, I., Scalable and deterministic fabrication of quantum emitter arrays from hexagonal boron nitride. *Nano Lett.* **2021,** *21* (8), 3626-3632.
10. Xu, X.; Martin, Z. O.; Sychev, D.; Lagutchev, A. S.; Chen, Y. P.; Taniguchi, T.; Watanabe, K.; Shalaev, V. M.; Boltasseva, A., Creating Quantum Emitters in Hexagonal Boron Nitride Deterministically on Chip-Compatible Substrates. *Nano Lett.* **2021,** *21* (19), 8182-8189.

11. Vogl, T.; Doherty, M. W.; Buchler, B. C.; Lu, Y.; Lam, P. K., Atomic localization of quantum emitters in multilayer hexagonal boron nitride. *Nanoscale* **2019,** *11* (30), 14362-14371.
12. Tan, Q.; Lai, J.-M.; Liu, X.-L.; Guo, D.; Xue, Y.; Dou, X.; Sun, B.-Q.; Deng, H.-X.; Tan, P.-H.; Aharonovich, I.; Gao, W.; Zhang, J., Donor–Acceptor Pair Quantum Emitters in Hexagonal Boron Nitride. *Nano Lett.* **2022,** *22* (3), 1331-1337.
13. Wang, L.; Papadopoulos, S.; Iyikanat, F.; Zhang, J.; Huang, J.; Taniguchi, T.; Watanabe, K.; Calame, M.; Perrin, M. L.; García de Abajo, F. J.; Novotny, L., Exciton-assisted electron tunnelling in van der Waals heterostructures. *Nature Mater.* **2023,** *22* (9), 1094-1099.
14. Horder, J.; White, S. J. U.; Gale, A.; Li, C.; Watanabe, K.; Taniguchi, T.; Kianinia, M.; Aharonovich, I.; Toth, M., Coherence Properties of Electron-Beam-Activated Emitters in Hexagonal Boron Nitride Under Resonant Excitation. *Physical Review Applied* **2022,** *18* (6), 064021.
15. Gale, A.; Li, C.; Chen, Y.; Watanabe, K.; Taniguchi, T.; Aharonovich, I.; Toth, M., Site-Specific Fabrication of Blue Quantum Emitters in Hexagonal Boron Nitride. *ACS Photonics* **2022**,9, 6, 2170–2177 .
16. Fournier, C.; Roux, S.; Watanabe, K.; Taniguchi, T.; Buil, S.; Barjon, J.; Hermier, J.-P.; Delteil, A., Two-Photon Interference from a Quantum Emitter in Hexagonal Boron Nitride. *Physical Review Applied* **2023,** *19* (4), L041003.
17. Zhigulin, I.; Yamamura, K.; Ivády, V.; Gale, A.; Horder, J.; Lobo, C. J.; Kianinia, M.; Toth, M.; Aharonovich, I., Photophysics of blue quantum emitters in hexagonal boron nitride. *Materials for Quantum Technology* **2023,** *3* (1), 015002.
18. Shevitski, B.; Gilbert, S. M.; Chen, C. T.; Kastl, C.; Barnard, E. S.; Wong, E.; Ogletree, D. F.; Watanabe, K.; Taniguchi, T.; Zettl, A.; Aloni, S., Blue-light-emitting color centers in high-quality hexagonal boron nitride. *Phys. Rev. B* **2019,** *100* (15), 155419.
19. Nonahal, M.; Horder, J.; Gale, A.; Ding, L.; Li, C.; Hennessey, M.; Ha, S. T.; Toth, M.; Aharonovich, I., Deterministic Fabrication of a Coupled Cavity–Emitter System in Hexagonal Boron Nitride. *Nano Lett.* **2023,** *23* (14), 6645-6650.
20. Koenderink, A. F., Single-Photon Nanoantennas. *ACS Photonics* **2017,** *4* (4), 710-722.
21. Wang, J.; Sciarrino, F.; Laing, A.; Thompson, M. G., Integrated photonic quantum technologies. *Nat. Photonics* **2020,** *14* (5), 273-284.
22. Hoang, T. B.; Akselrod, G. M.; Mikkelsen, M. H., Ultrafast Room-Temperature Single Photon Emission from Quantum Dots Coupled to Plasmonic Nanocavities. *Nano Lett.* **2016,** *16* (1), 270-275.
23. Akselrod, G. M.; Argyropoulos, C.; Hoang, T. B.; Ciracì, C.; Fang, C.; Huang, J.; Smith, D. R.; Mikkelsen, M. H., Probing the mechanisms of large Purcell enhancement in plasmonic nanoantennas. *Nat. Photonics* **2014,** *8* (11), 835-840.
24. Bogdanov, S. I.; Boltasseva, A.; Shalaev, V. M., Overcoming quantum decoherence with plasmonics. **2019,** *364* (6440), 532-533.
25. Bogdanov, S. I.; Shalaginov, M. Y.; Lagutchev, A. S.; Chiang, C.-C.; Shah, D.; Baburin, A. S.; Ryzhikov, I. A.; Rodionov, I. A.; Kildishev, A. V.; Boltasseva, A.; Shalaev, V. M., Ultrabright Room-Temperature Sub-Nanosecond Emission from Single Nitrogen-Vacancy Centers Coupled to Nanopatch Antennas. *Nano Lett.* **2018,** *18* (8), 4837-4844.
26. Dowran, M.; Butler, A.; Lamichhane, S.; Erickson, A.; Kilic, U.; Liou, S.-H.; Argyropoulos, C.; Laraoui, A., Plasmon Enhanced Quantum Properties of Single Photon Emitters with Hybrid Hexagonal Boron Nitride Silver Nanocube Systems. *Adv. Opt. Mater.* **2023,** *11* (16), 2300392.
27. Tran, T. T.; Wang, D. Q.; Xu, Z. Q.; Yang, A. K.; Toth, M.; Odom, T. W.; Aharonovich, I., Deterministic Coupling of Quantum Emitters in 2D Materials to Plasmonic Nanocavity Arrays. *Nano Lett.* **2017,** *17* (4), 2634-2639.
28. Xu, X.; Solanki, A. B.; Sychev, D.; Gao, X.; Peana, S.; Baburin, A. S.; Pagadala, K.; Martin, Z. O.; Chowdhury, S. N.; Chen, Y. P.; Taniguchi, T.; Watanabe, K.; Rodionov, I. A.; Kildishev, A. V.; Li, T.; Upadhyaya, P.; Boltasseva, A.; Shalaev, V. M., Greatly

Enhanced Emission from Spin Defects in Hexagonal Boron Nitride Enabled by a Low-Loss Plasmonic Nanocavity. *Nano Lett.* **2023,** *23* (1), 25-33.
29. Mendelson, N.; Ritika, R.; Kianinia, M.; Scott, J.; Kim, S.; Fröch, J. E.; Gazzana, C.; Westerhausen, M.; Xiao, L.; Mohajerani, S. S. J. A. M., Coupling spin defects in a layered material to nanoscale plasmonic cavities. **2022,** *34* (1), 2106046.
30. Cai, H.; Ru, S.; Jiang, Z.; Eng, J. J. H.; He, R.; Li, F.-l.; Miao, Y.; Zúñiga-Pérez, J.; Gao, W., Spin Defects in hBN assisted by Metallic Nanotrenches for Quantum Sensing. *Nano Lett.* **2023,** *23* (11), 4991-4996.
31. Cheng, P.-J.; Huang, Z.-T.; Li, J.-H.; Chou, B.-T.; Chou, Y.-H.; Lo, W.-C.; Chen, K.-P.; Lu, T.-C.; Lin, T.-R., High-Performance Plasmonic Nanolasers with a Nanotrench Defect Cavity for Sensing Applications. *ACS Photonics* **2018,** *5* (7), 2638-2644.
32. Knight, M. W.; King, N. S.; Liu, L.; Everitt, H. O.; Nordlander, P.; Halas, N. J., Aluminum for Plasmonics. *ACS Nano* **2014,** *8* (1), 834-840.
33. Wang, Z.; Dong, Z.; Gu, Y.; Chang, Y.-H.; Zhang, L.; Li, L.-J.; Zhao, W.; Eda, G.; Zhang, W.; Grinblat, G.; Maier, S. A.; Yang, J. K. W.; Qiu, C.-W.; Wee, A. T. S., Giant photoluminescence enhancement in tungsten-diselenide–gold plasmonic hybrid structures. *Nat. Commun.* **2016,** *7* (1), 11283.
34. Xu, J.; Dong, Z.; Asbahi, M.; Wu, Y.; Wang, H.; Liang, L.; Ng, R. J. H.; Liu, H.; Vallée, R. A. L.; Yang, J. K. W.; Liu, X., Multiphoton Upconversion Enhanced by Deep Subwavelength Near-Field Confinement. *Nano Lett.* **2021,** *21* (7), 3044-3051.
35. McPeak, K. M.; Jayanti, S. V.; Kress, S. J. P.; Meyer, S.; Iotti, S.; Rossinelli, A.; Norris, D. J., Plasmonic Films Can Easily Be Better: Rules and Recipes. *ACS Photonics* **2015,** *2* (3), 326-333.